



Article

Combination of Phase Change Composite Material and Liquid-Cooled Plate Prevents Thermal Runaway Propagation of High-Specific-Energy Battery

Weigao Ji, Yongchun Dang, Yongchao Yu, Xunli Zhou and Lei Li *

National Engineering Research Center of Electric Vehicles, Beijing Institute of Technology, Beijing 100081, China; jiweigaomail@163.com (W.J.); dangyongchun1@163.com (Y.D.); 3120230343@bit.edu.cn (Y.Y.); 3220240547@bit.edu.cn (X.Z.)

* Correspondence: flytolilei@bit.edu.cn

Abstract: Ternary lithium-ion batteries (LIBs) have the advantages of high energy density and high charging efficiency, and they are the preferred energy source for long-life new energy vehicles. However, when thermal runaway (TR) occurs in the ternary LIB, an open flame is easily produced. The burning phenomenon is intense, and the rapid of TR propagation is high; consequently, vehicle-level fire accidents are easily induced. These accidents have become the biggest obstacle restricting the batteries' development. Therefore, this study investigates the TR behavior of ternary LIBs at the cell and module levels. The addition of an insulation layer alone, including ceramic nano fibers, glass fiber aerogel, and phase-change composite materials, cannot prevent TR propagation. To completely block the TR propagation, we developed a safety prevention strategy, combining the phase-change composite materials with a commercial liquid cooling plate. This approach provides a three-level TR protection mechanism that includes heat absorption, heat conduction, and heat insulation. The use of a 2 mm thick phase change composite material combined with a liquid cooling plate effectively prevents the TR propagation between 60 Ah ternary LIBs with 100%SOCs. The front surface temperature of the adjacent cell is maintained near 90 °C, with its maximum temperature consistently stays below 100 °C. This study successfully demonstrates the blockage of TR propagation and offers valuable insights for the thermal safety design of high-specific-energy LIBs; the aim is to improve the overall safety of battery packs in practical applications.

Keywords: ternary lithium-ion batteries; thermal runaway propagation; numerical simulation; thermal propagation barrier



Academic Editor: Andrea Frazzica

Received: 22 December 2024

Revised: 20 January 2025

Accepted: 23 January 2025

Published: 26 January 2025

Citation: Ji, W.; Dang, Y.; Yu, Y.; Zhou, X.; Li, L. Combination of Phase Change Composite Material and Liquid-Cooled Plate Prevents Thermal Runaway Propagation of High-Specific-Energy Battery. *Appl. Sci.* **2025**, *15*, 1274. <https://doi.org/10.3390/app15031274>

Copyright: © 2025 by the authors. Licensee MDPI, Basel, Switzerland. This article is an open access article distributed under the terms and conditions of the Creative Commons Attribution (CC BY) license (<https://creativecommons.org/licenses/by/4.0/>).

1. Introduction

With the rapid development of the new energy vehicle industry, the safety problem of lithium-ion batteries (LIBs) has become increasingly prominent [1]. A new energy vehicle (NEV) may catch fire during driving and charging or while parked. Accident investigations have found that NEV fires can be caused by a variety of factors, including battery overcharging, a short circuit, or an external high-temperature environment [2–4]. As the market currently favors new energy vehicles with a high-purity electric range, vehicle manufacturers have launched models equipped with large-capacity and high-energy-density ternary LIBs. In the charged state, the high reactivity of the anode (LiC_x) results in a high level of safety risk for LIBs when exposed to elevated temperatures, overcharging/discharging, and physical damage. These abuse conditions can trigger

thermal runaway (TR) in single LIBs, leading to a cascading TR propagation with a range of hazardous consequences including swelling, fires, and even explosions [5–7]. Once a fire accident occurs, the harm caused by this model is significantly higher than that of models equipped with lithium-ion iron phosphate batteries. Therefore, improving the safety performance of cells and reducing the risk of heat spread between cells are the keys to reducing the harm caused by such accidents. By strengthening the fire isolation measures inside the battery system and optimizing the cooling technology, the triggering and spreading process of TR can be effectively delayed; then, the open flame can be effectively suppressed to prevent an explosion [8].

At the present stage, the strong randomness and complexity of the TR trigger determine the inevitability of a TR accident; thus, the delay scheme to prevent TR expansion is very important. NIU et al. [9] proposed the use of flame-retardant phase change materials and low thermal conductivity materials to delay the TR expansion of LIBs. The TR tests on battery modules demonstrate that the materials between batteries can efficiently inhibit the spread of TR, maintaining the maximum external temperature of the neighboring battery below 182.6 °C. WENG et al. [10] confirmed that aerogel felt with flame-retarded phase change material could effectively delay the TR expansion of LIBs. WILKE et al. [11] used composite phase change materials to block the TR expansion between 2.85 Ah 18650 cells induced by needle puncture. BECHER et al. [12] used aramid honeycomb and hydrogel materials to develop a thermal insulation layer that could be placed between individual batteries; this layer blocked the TR propagation between 37 Ah and NCM111 LIBs triggered by needle puncture. In previous studies, researchers also developed flexible ceramic insulation materials [13], flame-retardant phase change composite materials [14], hydrogel composite materials [15], and other intelligent barrier materials; these materials inhibit or block the TR between different types of lithium-ion batteries by functioning as thermal insulation barrier materials. In addition, the researchers also studied the methods of delaying TR propagation from the perspective of cooling and fire [16–18] extinguishing, which involved foam [17], fine water mist [19], liquid nitrogen [20], difluorodichloromethane [21,22], perfluorohex [23], anone, heptafluoropropane, dry ice [22], and other fire extinguishing agents. These agents were analyzed to determine their fire extinguishing effects on the battery fire and the harm of the material itself to the environment, and certain research results were obtained.

However, at present, there is no effective solution to the problem of the TR propagation of high-specific-energy, pouch batteries, such as ternary LIBs; therefore, this study carried out TR research on ternary LIB monomers, modules, and vehicles and obtained the law of TR and its spread. Furthermore, this study explored the passive safety protection method of TR at the battery module level and developed a new phase change composite material. The phase change composite material is based on ceramic nanofiber and is combined with the phase change material using adsorption; it demonstrates excellent heat absorption and heat insulation performance. The material and the liquid cooling plate jointly block the TR propagation, forming a three-level TR timing protection method: heat absorption-conduction-insulation. The evolution process of the thermal spread parameters, such as temperature change, maximum temperature, and propagation time, is analyzed.

2. Materials and Methods

2.1. Study on TR Temperature Characteristics of Cells

An NCM622 pouch cell (manufactured by Do-Fluoride New Energy Co., Ltd., Jiaozuo, China) with a nominal capacity of 60 Ah was used in the experiment. The detailed specifications are shown in Table 1.

Table 1. Pouch cell information.

Serial Number	Items	Specifications
1	Rated capacity	60 Ah @1 C, 25 °C
2	Nominal voltage	3.66 V @1 C, 25 °C
3	Standard charging	0.33 C CC-CV to 4.3 V, cutoff 0.05 C
4	Standard discharge	0.33 C CC to 2.8 V
5	Charge cut-off voltage	4.3 V
6	Discharge cut-off voltage	2.8 V
7	Single battery weight	830 ± 15 g
8	Energy density	≥270 Wh kg ⁻¹ , ≥570 Wh L ⁻¹
9	Dimensions	313 mm × 101 mm × 12 mm

Before the experiment, a cyclic charge and discharge instrument was used to cyclically pre-treat the battery cell; this process included the following steps. (1) A 0.5 C constant current charge was used to reach 4.3 V. (2) The constant voltage charge was switched until the charging current dropped to 200 mA. (3) The charging was stopped, and the cell was left to stand for 5 min. (4) Constant discharge at 0.5 C was conducted. (5) The above steps were repeated for the pre-cycle treatment of the 2.8 V to 4.3 V voltage range; the process was conducted twice. (6) Finally, the cell was charged to 100% SOC. In the pre-treatment process, it is necessary to ensure that the discharge capacity change in the cell is not higher than 3% of the rated capacity specified in the standard GB38031 [24].

As shown in Figure 1a, to investigate the temperature response of batteries under thermal abuse, we conducted ARC experiments. The 300 W heating source was used to heat the battery on one side to trigger TR, and the experimental setting is shown in Figure 1b. The battery was close to the heating plate of the same size and shape and was placed above the heat insulation plate. The ARC mainly tests the thermal characteristics of cells according to the “heat-wait-search” rule. In order to accurately monitor the battery’s temperature change, multiple K-type thermocouples are arranged on the surface of the battery, as shown in Figure 1c. The accuracy of the K-type thermocouples used in this study is specified as ±1.5 °C, which ensures reliable temperature measurements within the specified range. When the surface temperature of the battery reaches the preset target value, the resistance wire stops heating, and the experiment enters the “wait-search” stage. In this phase, the experiment mainly monitors whether the battery is able to maintain its temperature or whether the battery shows signs of temperature increase. If the temperature rise rate of the battery is detected at or above 0.02 °C min⁻¹, this usually indicates that the battery has started to generate its own heat; that is, there may be a slight failure inside the battery. In order to simulate the adiabatic environment during the self-generating phase, the ARC adjusts the heating power of the resistance wire to ensure that the air temperature in the calorimetric chamber is consistent with the surface temperature of the battery. This setting helps to ensure that the battery does not exchange heat with the outside world and that it more accurately simulates and analyzes the TR behavior that may occur in the battery under real use conditions. The entire process continues until the battery TR process naturally ends.

The TR heat generation model can be built according to the TR side reaction mechanism of the battery, and its accuracy can be verified by the experimental results. The TR chemical reaction includes 7 main processes: SEI film decomposition, negative electrode and electrolyte reaction, separator decomposition, electrolyte decomposition, positive electrode decomposition, large-scale internal short circuit, and adhesive decomposition. Under normal working conditions, the separator can block electrons. When the TR progress to the separator collapses, electrons and lithium ions are present at the same time in the positive and negative electrode shuttle. A large-scale internal short circuit is formed, which releases a lot of heat, leading to the occurrence of other reactions. The thermal model parame-

ters are shown in Table 2. The TR model of the LIB cell was established using COMSOL Multiphysics (v.6.3) according to the parameter table and the model principle [25].

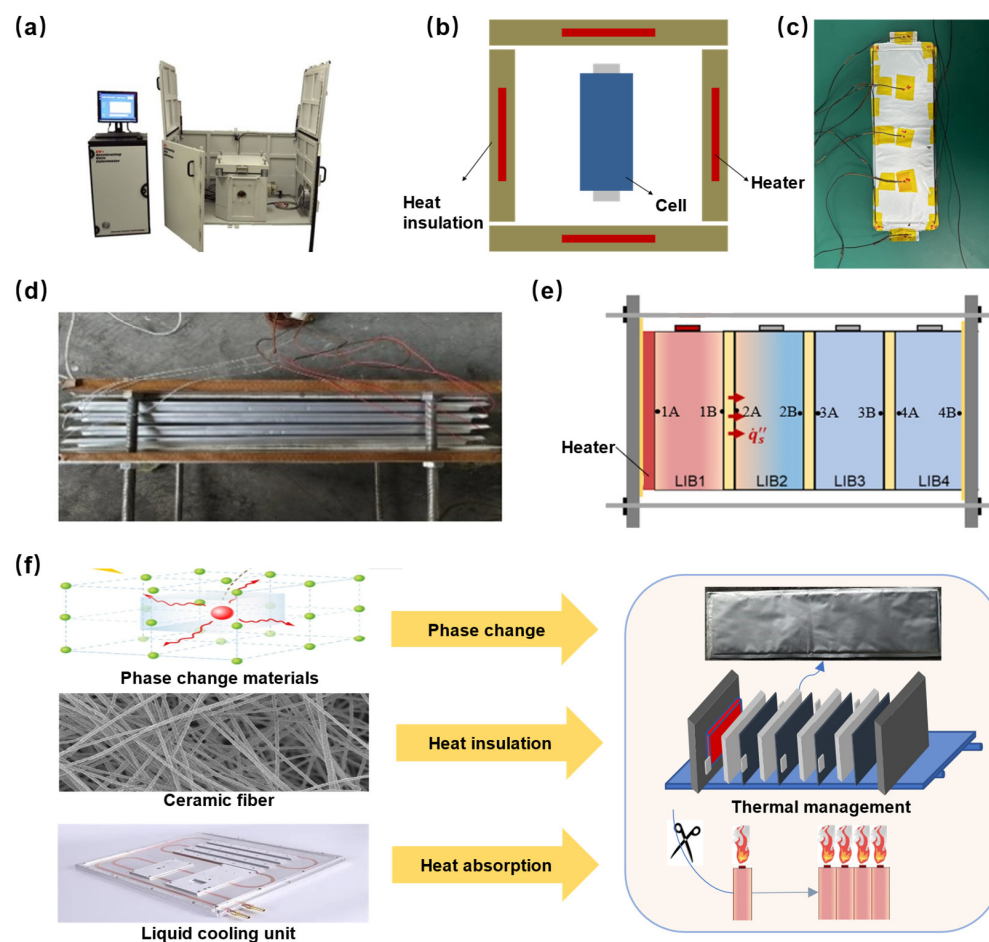


Figure 1. (a) Accelerating rate calorimeter (ARC); (b) schematic diagram of the single cell arrangement method used in the test; (c) battery image before test; (d) TR propagation test device; (e) schematic diagram of thermocouple arrangement; (f) schematic diagram of the overall principle and arrangement of the experiment.

Table 2. Parameters of TR model.

Material (180 °C Exothermic Peak)	$A_x/(s^{-1})$	m_x/g	$\Delta H_x/(J \cdot g^{-1})$	$c_{x,0}$	
SEI membrane	1.61×10^{15}	182	245	0.14	
Negative pole	$0.003 (T < 150 \text{ } ^\circ\text{C})$ 2.5×10^{14} $(T \geq 150 \text{ } ^\circ\text{C})$	180	1805	1.00	
Separator	1.5×10^{40}	20	−213	1.00	
Electrolyte	3×10^{15}	137	680	1.00	
Positive electrode	1.75×10^9 1.077×10^{12}	285 285	75 88	0.99 0.99	
Material (220 °C exothermic peak)	$E_{a,x}/(J \cdot mol^{-1})$	N	m	f (x)	$T_0/^\circ\text{C}$
SEI film	1.3×10^{15}	1	0	1	80
Negative electrode	2.3×10^4	1	0	1	80
Separator	4.22×10^5	1	0	1	130
Electrolyte	1.65×10^5	1	0	1	130
Positive electrode	1.15×10^5 1.6×10^5	1 1	1 1	1 1	140 161

2.2. Study on TR Temperature Characteristics of Battery Modules

The constructed experimental system consists of a battery module composed of four ternary LIBs (NCM622), two mica plates, a heater, and stainless steel fixtures, as shown in Figure 1d. The two mica plates are placed between the two sides of the module and the fixture to prevent heat loss. The heater power is 300 W, and the battery TR is triggered by side heating. The data measurement and acquisition system consists of a data acquisition instrument, a camera, and a thermocouple, and the sampling frequency of the data acquisition instrument is 1 s. Because the TR of the ternary LIB is to be accompanied by a very violent explosion and fire phenomenon, the battery module is placed in the explosion-proof box during the experiment in order to protect the equipment and personal safety. The specific steps for the pre-treatment of the battery before the experiment are as follows: first, it is left to stand for 30 min; then, the constant discharge, constant current, and constant voltage charging cycle is carried out twice; finally, it is charged to 100% SOC. In the study of TR propagation between battery modules without insulation materials, the battery module is equipped with 4 temperature measurement points, which are located in the center of each interface of the battery unit.

Based on the actual parameters of the battery, a three-dimensional physical model and a one-dimensional heat transfer model of the cell are established in this study. The model consists of a heater and four cells. Firstly, a heat source with a power of 300 W is applied to the wall of the 3D physical model to simulate heating and calculate the temperature, and the temperature is averaged in a specified section. Then, the specified cross-section feeds the temperature back to the one-dimensional TR model, and the one-dimensional TR model judges whether the TR is triggered and calculates the TR heat production according to the temperature. The TR heat production is then fed back to the three-dimensional physical model, and the process is repeated until the TR is over. On this basis, the TR propagation model of the battery module adds the heat transfer process between the cells and the external environment, which is composed of four cell models arranged without spacing. The parameters of the boundary conditions are shown in Table 3.

Table 3. Parameters of the boundary conditions.

Mode	Description	δ (mm)	λ (W·m ⁻¹ ·K ⁻¹)	h (W·m ⁻² ·K ⁻¹)	ϵ
Heat conduction	Heater—Battery thermal resistance layer	0.01	0.023	/	/
	Shell—Core thermal resistance layer	0.01	0.023	/	/
	Outer shell—Outer shell thermal resistance layer	0.10	0.010	/	/
Heat convection	Shell—Polar bear thermal barrier layer	0.01	0.023	/	/
	Surface radiant heat transfer	/	/	20	/
Heat radiation	Surface convection heat transfer	/	/	/	0.04

2.3. TR Propagation Barrier Method with Only Insulation Layer Added

The experiment was carried out in the 4-cell battery module. Three types of heat insulation materials, a, b, and c, with the same size and 3 mm thickness were set between the adjacent cells and secured with a fixture plate. The interface between the cell and the heat insulation material was still arranged with No. 1–8 K-type thermocouples to characterize the temperature distribution on the surface of the cell, as shown in Figure 1e.

TR propagation between batteries is mainly realized through wall heat conduction. In order to slow down or even cut off such propagation, a scheme involving the addition of a thermal insulation layer between the adjacent cells was proposed. To this end, a variety

of thermal insulation materials, including a glass aerogel plate and a nano-ceramic fiber board, were considered, and the TR propagation test was carried out to compare the barrier effects. However, the heat insulation measures may lead to the accumulation of heat in the battery module, which is contrary to the demand for heat dissipation in the normal operation of the battery system and thus affects the thermal management of the battery module under conventional working conditions.

Therefore, a self-developed composite phase change material was selected; it was prepared using nano-ceramic fiber substrate material and phase change endothermic material. The substrate consists of silica nanofiber mats and supporting materials. The phase change materials include one or more silica sol, aluminum sol, and saturated calcium chloride solutions. The flame retardant materials include phosphorus-based flame retardants, such as SCCS, triethyl phosphate, and triphenyl phosphate. Our phase change material contains both phase change materials and insulating substrates, offering a high phase change enthalpy value (1800–2200 J g⁻¹). During TR, it effectively absorbs energy through both the thermal insulation properties of the material and the phase transition of the phase change materials, playing a significant role in blocking heat propagation. Nano-ceramic fiber has excellent thermal insulation performance and can withstand high-temperature environments; thus, it is highly suitable for the protection of battery TR. The composite phase change layer used in the TR propagation barrier test carried out in this section absorbs calcium chloride solution, and it was tested and compared with the nano-ceramic fiber and glass fiber aerogel insulation layer; the same 2 mm thickness was used to carry out the TR propagation test and to analyze their TR barrier effects.

In addition, the main raw materials of the phase change material are nanosilica and silica sol. Studies have shown that nanosilica currently poses no threat to aquatic organisms in surface waters [26]. Silica sol is a purely mineral-based product with adhesive and neutralizing properties for certain pollutants. This makes it suitable for soil stabilization and the neutralization of heavy metal ions and other contaminants in soil [27]. Overall, our phase change material demonstrates excellent environmental friendliness and sustainability.

2.4. Heat Absorption–Conduction–Insulation TR Sequential Protection Method

From the TR propagation experiment presented above, it can be seen that regardless of whether the heat insulation materials are those commonly used in the industry (nanofibers, aerogels) or whether the application of phase change materials for heat absorption only occurs in the early stage of the TR, the 60 Ah terpolymer LIB in this test cannot achieve thermal blocking. This shows that relying on thermal insulation materials may not be sufficient to completely prevent the 60 Ah ternary LIB combustion and diffusion and that it is also necessary to combine other measures to guide the heat out of the battery system and comprehensively improve the safety of the battery system. In addition, although the phase change heat release method has a better barrier effect, the amount of phase change materials is limited and cannot cope with the huge heat released by the battery module of this test.

Therefore, a method of blocking runaway thermal spread based on liquid cooling system and composite phase change materials is proposed in this study. In addition to the use of a composite phase change insulation layer, a liquid cooling plate is placed at the bottom of the battery module. The size of the cooling plate is 400 × 125 × 15 mm, with a water channel diameter of 10 mm. The coolant is water, the flow rate is set to 0.1 L s⁻¹, and the initial temperature is 20 °C (room temperature). When the experiment begins, the liquid cooling system and the heater are started at the same time. After the first battery is out of control, the heater is disconnected, and the liquid cooling system continues to work. The overall principle and the arrangement of the experiment are shown in Figure 1f.

3. Results

3.1. TR Heat Production Process and Model Verification of Battery Cells

As shown in Figure 2a, based on the temperature change profile of the battery, the evolution process of battery TR can be roughly divided into four key stages. In stage I (from room temperature to 84 °C), the temperature rise in the battery is mainly caused by the heating action of the ARC; no significant exothermic chemical reaction occurs inside the battery, and the overall state is still stable. Entering stage II, when the temperature reaches 84 °C, the SEI film of the battery begins to decompose, resulting in direct contact between the electrolyte and the graphite negative electrode, triggering a reaction. Alkane-like gases begin to be produced inside the battery, resulting in a slight expansion of the battery. In stage III (from 84 °C to 147 °C), the separator begins to shrink and melt due to the high temperature; consequently, the positive and negative poles of the battery may then contact locally, triggering the internal short circuit; the separator contraction leads to a large-scale short circuit inside the battery, and the temperature rise rate of the battery is significantly accelerated. Finally, stage IV (above 147 °C) marks the entry of the battery into the TR stage; a series of thermal reactions are triggered, and the temperature spikes from 157.6 °C to 660 °C in a very short time. This is mainly due to the rapid consumption of materials inside the battery and the violent release of heat from the chemical reaction. The characteristic TR temperature [5–7] of the single battery measured in this experiment is shown in Table 4.

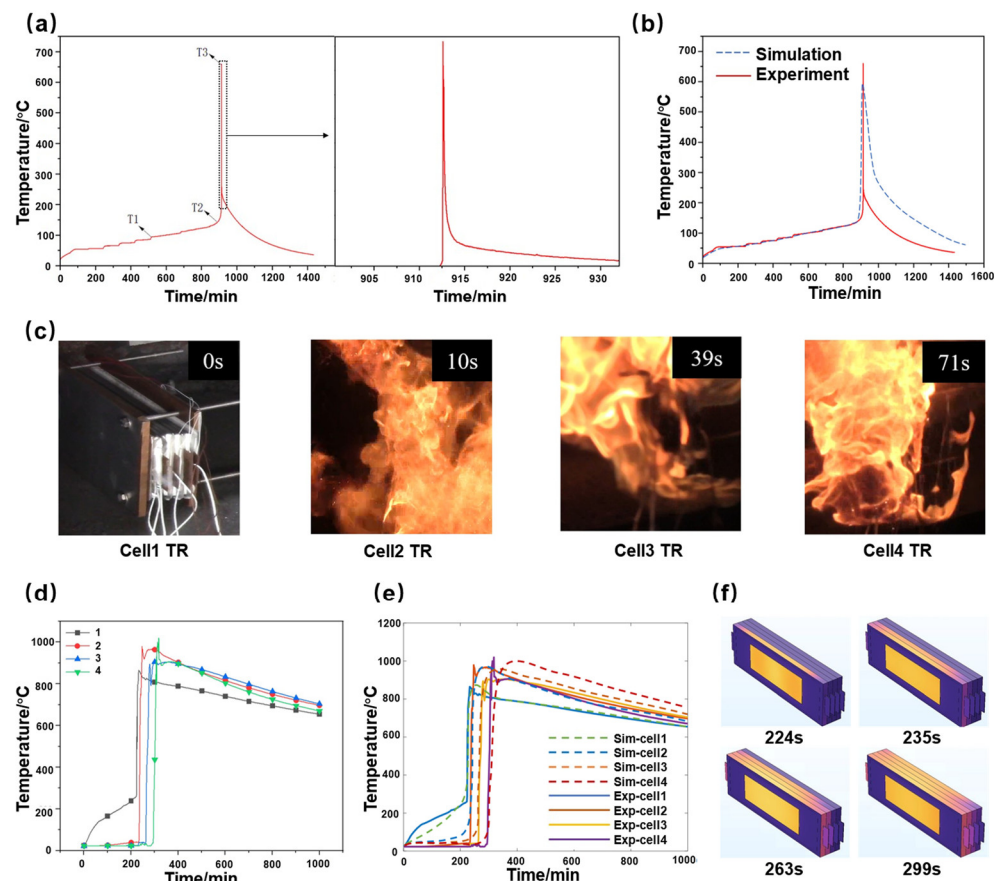


Figure 2. (a) The center temperature of the cell in the ARC experiment; (b) comparison of simulation and experimental results of ARC experiment; (c) battery module TR propagation process; (d) TR temperature of battery module with different insulation layers; (e) comparison of simulation and experimental results of TR propagation experiment; (f) the dynamic image of TR simulation.

Table 4. The characteristic temperature of TR.

T₁ (Temperature of Initiation of Autogenic Heat)	T₂ (TR Trigger Temperature)	T₃ (TR Maximum Temperature)
84 °C	147 °C	660 °C

The energy released by the battery directly affects the maximum temperature. It can be seen in Figure 2b that the accuracy of the maximum temperature of the model is 91.3%, which can accurately represent the energy characteristics of the battery TR; additionally, the temperature change trend in the whole TR process is well matched, which further proves the rationality of the model. In the final cooling process of the battery, the cooling conditions of the ARC during the test cannot be accurately obtained; the TR ends at this time, and this phase will not be discussed further.

3.2. TR Propagation Process and Model Verification of Battery Modules

The TR propagation process in the battery unit is composed of five main stages: exhaust, initial jet fire, jet fire diffusion, buoyancy fire, and extinction. In the battery module test process, when the TR occurs, it is usually observed that an intense jet flame from the cell is emitted. This phenomenon is particularly evident in the first cell to experience TR. However, when the exhaust phase occurs in the first cell, it is difficult to observe the exhaust phase in detail due to the extremely fast temperature rise in the other cells. This is mainly because as the temperature rises, the newly generated gas is immediately ignited by the flame of the previous cell. In addition, when the TR of the current cell has not fully entered the buoyancy fire stage, the initial flow fire of the adjacent cell begins to form due to the propagation of heat and flame from one cell to another. This chain reaction of TR leads to the possibility of TR in the cells inside the battery module, which further increases the safety risk. The TR propagation process of the battery module with different insulation materials is shown in Figure 2c.

The experiment failed to show gas production in the cell before TR. When the initial cell experienced TR, a large amount of smoke could be observed, accompanied by intense combustion. This is because there was an assembly force between the cells; the cell broke easily due to its coating material, an aluminum–plastic film. The gas production of the internal component materials was discharged with the initial phase of the flow of fire and did not accumulate in the battery; the occurrence of bulges resulted in the intense and very quick combustion of the battery. Therefore, in the TR propagation of the battery module, the initial time of the TR of a single cell was determined by observing the emergence of the jet fire. Figure 2d shows the change process of the temperatures of various surfaces of the cell over time.

The comparison of the simulation and test results is shown in Figure 2e, which indicates that the simulation results are basically consistent with the experimental results at the time when the battery triggers TR; this proves that the simulation model can accurately capture the behavior and propagation process of the battery TR and verifies the reliability and accuracy of the simulation model. The temperature field distribution of the model in the process of TR was observed using numerical simulation images, as shown in Figure 2f.

3.3. TR Propagation Barrier with Only Insulation Layer Added

The TR propagation time between cells is shown in Figure 3a, and the propagation test without the insulation layer is taken as the control group. The comparative analysis shows that the thermal propagation time of the module with the insulation layer is much longer than that of the module without the insulation layer. The effect of the glass fiber aerogel insulation layer is better than that of the nano-ceramic fiber insulation layer, while

the composite phase change insulation layer has the best effect, and its thermal spread inhibition effect is greatly improved compared with the first two materials. However, regardless of the kind of insulation layer that is used, the battery module has completed thermal spread; the difference is expressed in the spread time. The battery module of the composite phase change insulation layer demonstrates a good effect in restraining TR propagation. The thermal propagation test shows that the composite phase change insulation layer has good phase change heat absorption and heat insulation performance and that it can effectively delay the TR propagation of large-capacity ternary LIBs. In addition, under normal conditions, the composite phase change insulation material has good thermal conductivity, which further ensures its reliability and practicability.

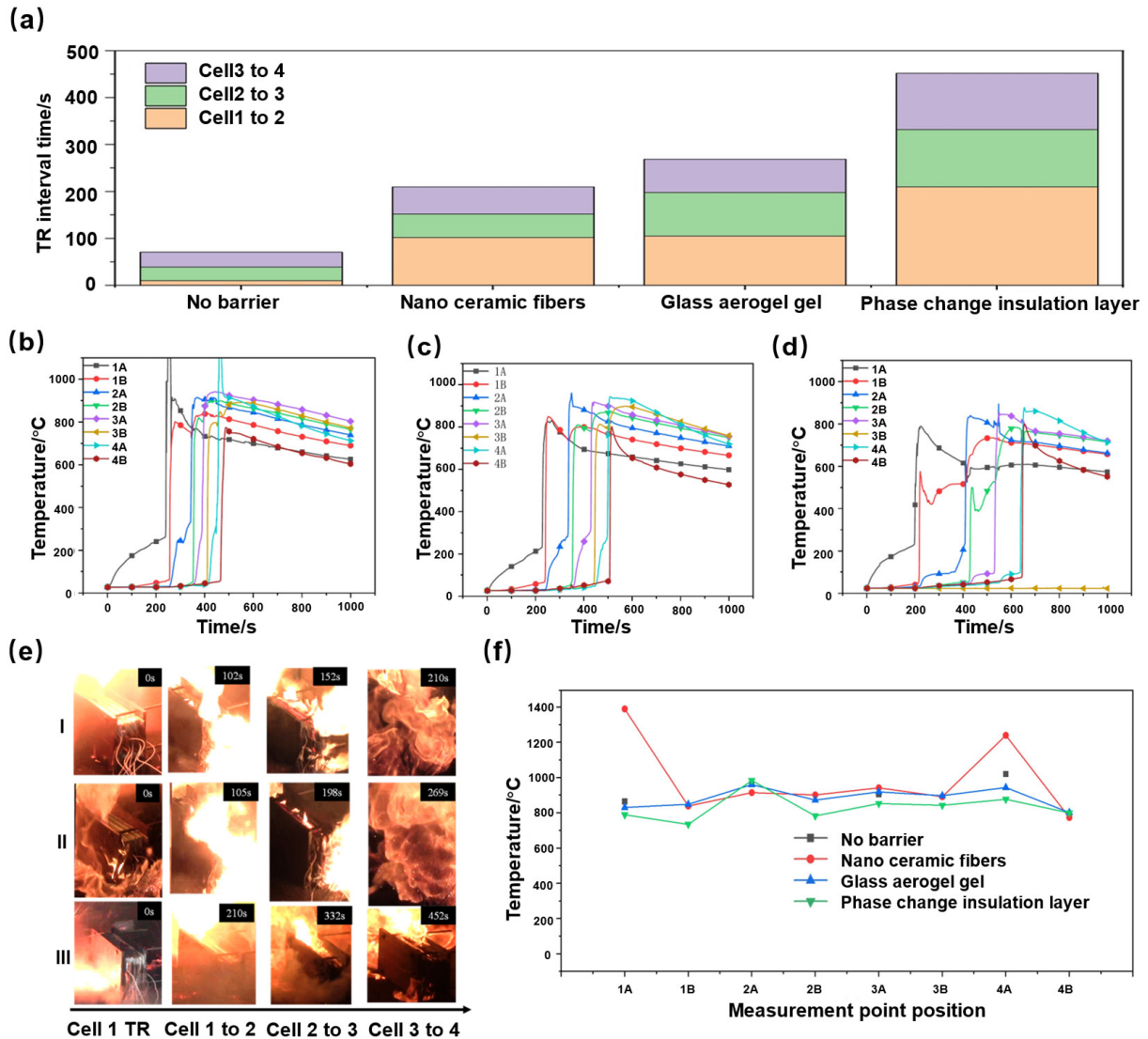


Figure 3. (a) Cell-to-cell TR propagation time; (b) TR temperature rise diagram of battery module using nano-ceramic fiber insulation layer; (c) TR temperature rise diagram of battery module using glass aerogel insulation layer; (d) TR temperature rise diagram of battery module using phase change insulation layer; (e) TR propagation phenomenon using different insulation layers; (f) maximum temperature at each measuring point.

The temperature characteristics of the different thermal insulation materials are shown in Figure 3b–d. According to the temperature characteristics diagram, the insulation layer of different materials has a significant influence on the heat spread between batteries. Compared with no barrier, as described in Section 2.1, when the nano-ceramic fiber insulation

layer and glass fiber aerogel insulation layer are used, the heat transfer between adjacent cells is delayed to a certain extent; the temperature that triggers TR is relatively high (280 °C), and the rise rate is slow. When the composite phase change material insulation layer is used, the phase change heat absorption occurs in the insulation layer, delaying the triggering of heat spread between the batteries; consequently, the second battery can maintain a low temperature within a certain period of time, which shows that the volatilization of the phase change material effectively reduces the surface temperature of the battery. With the consumption of phase change materials, the heat absorption layer cannot play a role. The temperature of the battery wall gradually rises to the TR triggering temperature, which triggers TR.

Figure 3e fully records the phenomenon that occurs when each cell in the battery module triggers TR. By observing the experimental phenomenon, it can be seen that when different insulation layers are used, the situation in which TR occurs in the first battery is different. In the nano-ceramic fiber insulation layer module and the glass fiber aerogel insulation layer module, when TR occurs, the locations of explosion and fire are located at different side poles; in the composite phase change material insulation layer battery module, a strong flame and a lot of smoke erupt from the bottom side of the first violent explosion, followed by the explosion of the other surfaces.

The maximum TR temperature measured at each temperature measuring point during the TR process is shown in Figure 3f. The maximum temperature characteristics of the thermal insulation layer experiment using different materials show that the temperature of the front surface is always higher than that of the back surface; this is because the front surface is affected by self-generated heat and lateral heating, while the back surface is only affected by self-generated heat. The addition of an insulation layer can reduce the maximum temperature in the TR process to some extent. When the composite phase change material is used as the insulation layer, the maximum temperature of the TR of the battery can be significantly reduced because the phase change material plays a role in heat absorption.

The physical images of the different thermal insulation materials are shown in Figure 4a, and the SEM images of the three materials are shown in Figure 4b. It can be seen from the SEM images that the diameter and thickness of the nano-ceramic fibers are different and that they have a crisscross distribution in space. The glass aerogels have dense fiber filaments, and they also fill a small amount of the aerogel particles between the fibers, which enhances their heat insulation ability. The composite phase change material has a large amount of liquid phase change and flame-retardant materials arranged between the nanofibers, which proves that it has a certain cooling and flame-retardant function when the TR occurs. The temperature–time relationship of the thermal diffusion of the different thermal insulation materials is shown in Figure 4c. The transient plane heat source method is used to measure thermal conductivity, and the thermal property parameters can be obtained using a mathematical model. The thermal conductivity in the thickness direction and the thermal diffusivity in the format direction of the composite phase change materials are superior to those of the other two materials, and it can be seen that the composite photo-materials have lower thermal conductivity in the vertical direction. The thermal diffusivity in the direction of the format is higher, which indicates its barrier performance for thermal diffusion between cells under TR conditions and its good heat dissipation performance under normal conditions.

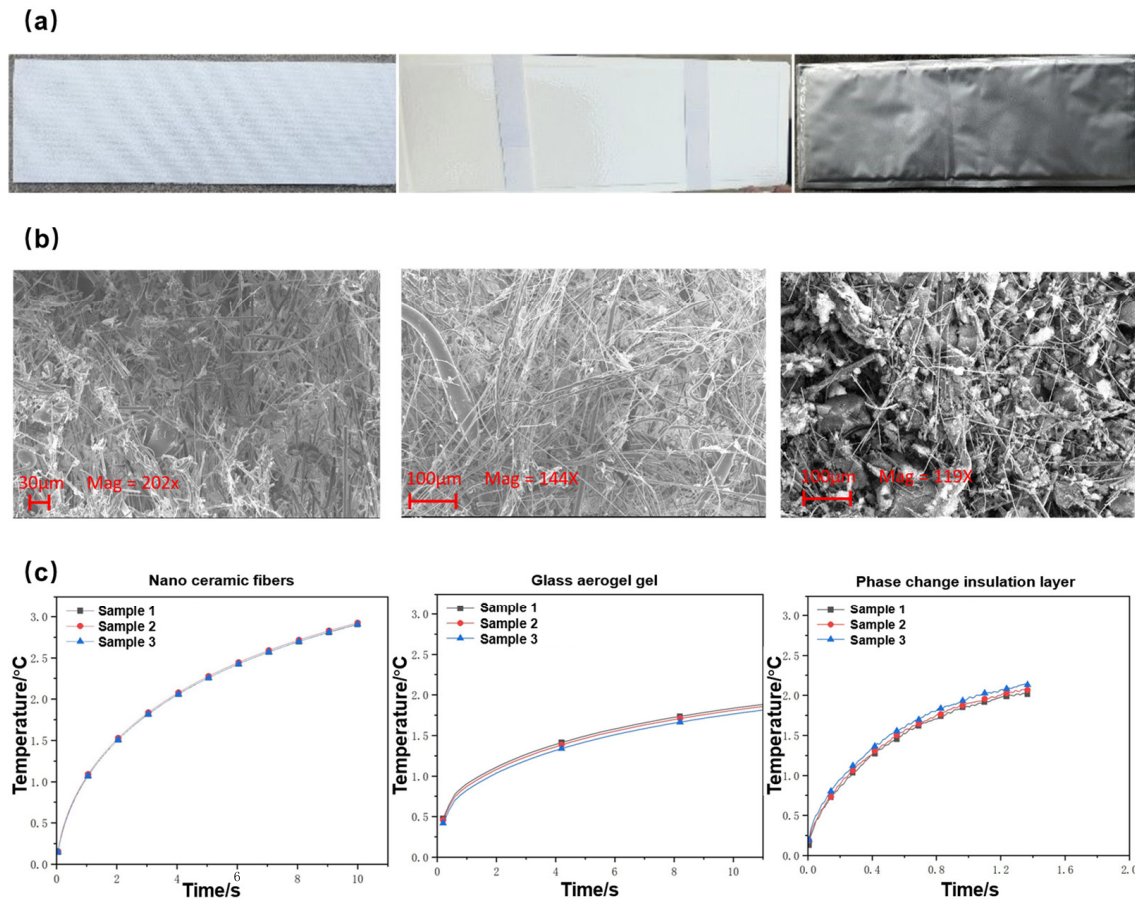


Figure 4. (a) The physical images of different thermal insulation materials; (b) the SEM images of the three materials; (c) the temperature–time relationship of thermal diffusion of different thermal insulation materials.

3.4. PCM and Liquid-Cooled Plate Block TR Propagation

Figure 5a shows the comparison between the TR blocking experiments with only phase change composites and the experiments with liquid-cooled plates combined with phase change composites. In the combined blocking experiment, the first battery lost thermal control and exploded, emitting flames and smoke. After the TR combustion of the first battery ended, there was still a small quantity of white smoke flowing out, but in the second battery and the subsequent batteries, the TR phenomenon did not occur.

Figure 5b shows the temperature characteristics of the TR propagation blocking experiment. When the composite phase change material insulation layer and the liquid cooling system worked together, the temperature of the first battery was slowly raised to about 400 °C by the action of the heater. After TR occurred, the surface temperature of the first battery suddenly rose to nearly 650 °C, and the rear surface suddenly rose to nearly 450 °C. At this time, due to the phase change endothermic effect of the composite phase change layer, the temperature of the front and back surfaces of the first section fell slightly, and the temperature of the front surface of the second battery was controlled at nearly 90 °C. After 100 s, with the consumption of the phase change materials, the composite phase change layer continued to have a heat insulation effect. After the front and back surfaces of the first battery reached the highest temperature, due to the existence of the thermal insulation layer, the speed of heat propagation to the second battery was significantly delayed, and the liquid cooling system could continue to cool the TR battery; the temperature continued to fall to below 250 °C, and the highest temperature of the front surface of the second battery was always maintained below 100 °C. The subsequent surface temperature of each battery

was always maintained at a low level, far below the critical temperature that triggers TR, and the TR propagation was successfully blocked.

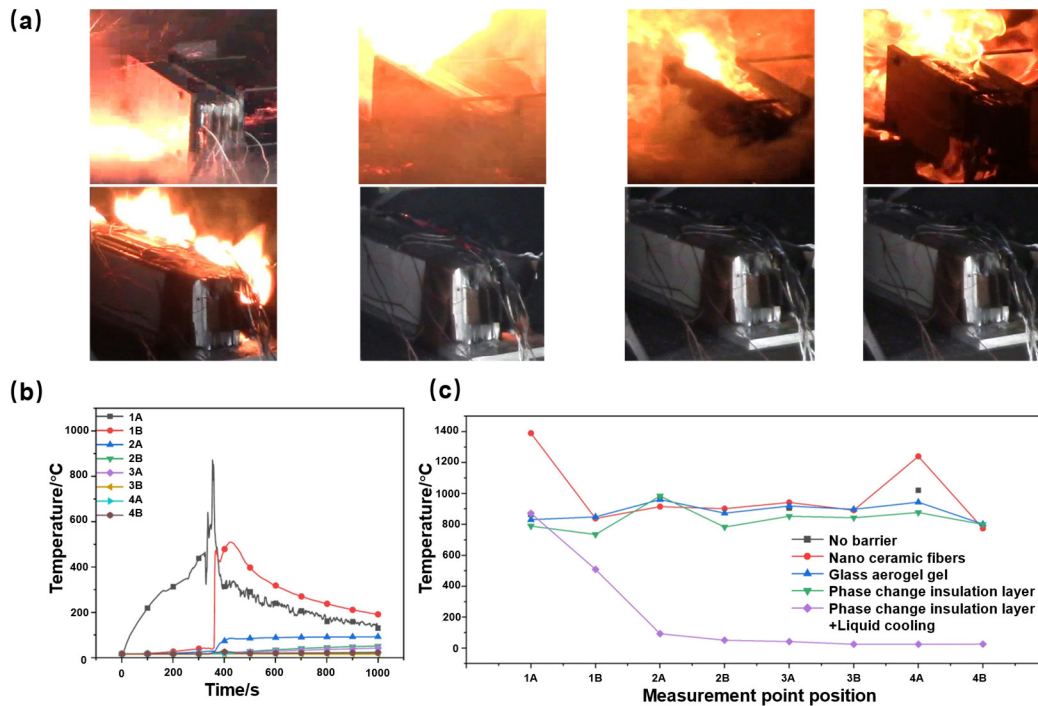


Figure 5. (a) Comparison of TR blocking experiments with only phase change composites and liquid-cooled plates combined with phase change composites; (b) the temperature characteristics of the TR propagation blocking experiment; (c) maximum temperature characteristic of the TR propagation blocking experiment and the comparison with the previous experiments.

Figure 5c shows the maximum temperature characteristic of the TR propagation blocking experiment and the comparison with the previous experiment. It can be seen in the figure that, due to the combined effect of the composite phase change layer and the liquid cooling system, the maximum temperature of the surface after the first cell is controlled at about 500 °C; the maximum temperature of the front surface of the second battery is always below 100 °C, and the maximum temperature of the other surfaces is below 50 °C, which is far below the critical temperature for triggering TR.

The safety prevention and control strategy integrates phase change composite materials with a liquid cooling plate. This approach does not require significant modifications to the existing protective structure of current new energy vehicles; instead, it only necessitates replacing the existing thermal insulation material with a new one. As a result, this strategy significantly reduces the cost associated with the adoption of new technologies and demonstrates high feasibility.

4. Conclusions

This study used the ternary LIB for vehicles as the research object. It carried out a TR test of a single LIB and a TR propagation test of a battery module, constructed a TR heat production model and a TR propagation model of a battery cell, summarized the TR heat generation behavior of a single battery and the TR propagation characteristics of a battery module, and verified the findings with the experimental results. According to the TR of the LIB and its propagation characteristics, a TR propagation blocking scheme was proposed and verified by the experiments. Finally, a TR blocking method for a ternary LIB module for the vehicle was proposed. The research work in this study provides valuable insights

for improving the safety of the power battery system of new energy vehicles. The main research contents and conclusions are as follows:

- (1) The TR behavior of the cells was studied, and the TR heat production model of the cells was established. A high-precision one-dimensional TR heat generation model of the cells was established; this model reflected the changing trend of parameters such as the TR propagation time and maximum temperature and revealed the TR mechanism of the cells.
- (2) An unhindered TR propagation test was carried out, and the TR propagation model of the LIB pack was established. The TR propagation law of the battery module was obtained through the TR propagation test of the unblocked battery module. Based on the heat transfer theory, combined with the total TR heat release measured in the ARC test of the battery unit, the TR propagation model of the battery module was established. The test results verified the accuracy and reliability of the model.
- (3) Based on the control variable method, the TR propagation barrier test and the TR propagation test of the nano-ceramic fiber, aerogel, and composite phase change insulation layer were carried out. The results show that the composite phase change material is superior to other materials with only heat insulation function in terms of the maximum temperature and spread time due to its phase change heat absorption ability. However, because the heat cannot be effectively transferred, only adding an insulation layer cannot significantly reduce the maximum TR temperature, and a single heat insulation measure cannot effectively inhibit the thermal spread of the ternary LIB module, as shown in this study.
- (4) A TR timing protection method based on thermal insulation with endothermic–thermal conductivity was proposed. To design a three-level TR sequential protection method involving “early heat absorption, middle heat conduction, late heat insulation”, this study used phase change materials in the initial phase of the TR phase change heat absorption; in addition, it used fire retardant materials and a liquid cooling system in the TR process of the rapid conduction of heat characteristics. The method was used to successfully block the 60 Ah terpolymer LIB module TR propagation.

Author Contributions: Methodology, W.J. and Y.Y.; Validation, W.J.; Investigation, Y.D. and X.Z.; Resources, L.L.; Writing—original draft, W.J.; Writing—review & editing, Y.D., Y.Y. and X.Z.; Supervision, L.L.; Funding acquisition, L.L. All authors have read and agreed to the published version of the manuscript.

Funding: This work was funded by the Zhejiang Province Science and Technology Program Grant (2024C0127(SD2)), National Key R&D Program of China under Grant 2023YFB2407900, the National Natural Science Foundation of China under Grant 52302512, and State Key Laboratory of New Ceramic and Fine Processing Tsinghua University No. KFZD202305.

Institutional Review Board Statement: Not applicable.

Informed Consent Statement: Not applicable.

Data Availability Statement: The original contributions presented in this study are included in the article. Further inquiries can be directed to the corresponding author.

Conflicts of Interest: The authors declare no conflicts of interest.

References

1. Yu, Q.; Nie, Y.; Peng, S.; Miao, Y.; Zhai, C.; Zhang, R.; Han, J.; Zhao, S.; Pecht, M. Evaluation of the safety standards system of power batteries for electric vehicles in China. *Appl. Energy* **2023**, *349*, 121674. [[CrossRef](#)]
2. Ren, D.; Hsu, H.; Li, R.; Feng, X.; Guo, D.; Han, X.; Lu, L.; He, X.; Gao, S.; Hou, J.; et al. A comparative investigation of aging effects on thermal runaway behavior of lithium-ion batteries. *eTransportation* **2019**, *2*, 100034. [[CrossRef](#)]

3. Wang, Q.; Ping, P.; Zhao, X.; Chu, G.; Sun, J.; Chen, C. Thermal runaway caused fire and explosion of lithium ion battery. *J. Power Sources* **2012**, *208*, 210–224. [[CrossRef](#)]
4. Spotnitz, R.; Franklin, J. Abuse behavior of high-power, lithium-ion cells. *J. Power Sources* **2003**, *113*, 81–100. [[CrossRef](#)]
5. Feng, X.; He, X.; Ouyang, M.; Lu, L.; Wu, P.; Kulp, C.; Prasser, S. Thermal runaway propagation model for designing a safer battery pack with 25 Ah LiNi Co Mn O₂ large format lithium ion battery. *Appl. Energy* **2015**, *154*, 74–91. [[CrossRef](#)]
6. Feng, X.; Ouyang, M.; Liu, X.; Lu, L.; Xia, Y.; He, X. Thermal runaway mechanism of lithium ion battery for electric vehicles: A review. *Energy Storage Mater.* **2018**, *10*, 246–267. [[CrossRef](#)]
7. Ren, D.; Feng, X.; Liu, L.; Hsu, H.; Lu, L.; Wang, L.; He, X.; Ouyang, M. Investigating the relationship between internal short circuit and thermal runaway of lithium-ion batteries under thermal abuse condition. *Energy Storage Mater.* **2021**, *34*, 563–573. [[CrossRef](#)]
8. Talele, V.; Patil, M.S.; Panchal, S.; Fraser, R.; Fowler, M. Battery thermal runaway propagation time delay strategy using phase change material integrated with pyro block lining: Dual functionality battery thermal design. *J. Energy Storage* **2023**, *65*, 107253. [[CrossRef](#)]
9. Niu, J.; Deng, S.; Gao, X.; Niu, H.; Fang, Y.; Zhang, Z. Experimental study on low thermal conductive and flame retardant phase change composite material for mitigating battery thermal runaway propagation. *J. Energy Storage* **2022**, *47*, 103557. [[CrossRef](#)]
10. Weng, J.; Ouyang, D.; Yang, X.; Chen, M.; Zhang, G.; Wang, J. Alleviation of thermal runaway propagation in thermal management modules using aerogel felt coupled with flame-retarded phase change material. *Energy Convers. Manag.* **2019**, *200*, 112071. [[CrossRef](#)]
11. Wilke, S.; Schweitzer, B.; Khateeb, S.; Al-Hallaj, S. Preventing thermal runaway propagation in lithium ion battery packs using a phase change composite material: An experimental study. *J. Power Sources* **2017**, *340*, 51–59. [[CrossRef](#)]
12. Becher, D.; Bauer, M.; Döring, H.; Böse, O.; Friess, B.; Danzer, M.A. Preventing thermal propagation in battery packs using enthalpy supported thermal barriers. *J. Energy Storage* **2021**, *42*, 103057. [[CrossRef](#)]
13. Li, L.; Jia, C.; Liu, Y.; Fang, B.; Zhu, W.; Li, X.; Schaefer, L.; Li, Z.; Zhang, F.; Feng, X.; et al. Nanograin–glass dual-phasic, elasto-flexible, fatigue-tolerant, and heat-insulating ceramic sponges at large scales. *Mater. Today* **2022**, *54*, 72–82. [[CrossRef](#)]
14. Li, L.; Xu, C.; Chang, R.; Yang, C.; Jia, C.; Wang, L.; Song, J.; Li, Z.; Zhang, F.; Fang, B.; et al. Thermal-responsive, super-strong, ultrathin firewalls for quenching thermal runaway in high-energy battery modules. *Energy Storage Mater.* **2021**, *40*, 329–336. [[CrossRef](#)]
15. Li, L.; Fang, B.; Ren, D.; Fu, L.; Zhou, Y.; Yang, C.; Zhang, F.; Feng, X.; Wang, L.; He, X.; et al. Thermal-Switchable, Trifunctional Ceramic–Hydrogel Nanocomposites Enable Full-Lifecycle Security in Practical Battery Systems. *ACS Nano* **2022**, *16*, 10729–10741. [[CrossRef](#)] [[PubMed](#)]
16. Wang, K.; Ouyang, D.; Qian, X.; Yuan, S.; Chang, C.; Zhang, J.; Liu, Y. Early Warning Method and Fire Extinguishing Technology of Lithium-Ion Battery Thermal Runaway: A Review. *Energies* **2023**, *16*, 2960. [[CrossRef](#)]
17. Lv, Y.; Geng, X.; Luo, W.; Chu, T.; Li, H.; Liu, D.; Cheng, H.; Chen, J.; He, X.; Li, C. Review on influence factors and prevention control technologies of lithium-ion battery energy storage safety. *J. Energy Storage* **2023**, *72*, 108389. [[CrossRef](#)]
18. Li, X.; Zhang, M.; Zhou, Z.; Zhu, Y.; Du, K.; Zhou, X. A novel dry powder extinguishant with high cooling performance for suppressing lithium ion battery fires. *Case Stud. Therm. Eng.* **2023**, *42*, 102756. [[CrossRef](#)]
19. Liu, T.; Tao, C.; Wang, X. Cooling control effect of water mist on thermal runaway propagation in lithium ion battery modules. *Appl. Energy* **2020**, *267*, 115087. [[CrossRef](#)]
20. Huang, Z.; Liu, P.; Duan, Q.; Zhao, C.; Wang, Q. Experimental investigation on the cooling and suppression effects of liquid nitrogen on the thermal runaway of lithium ion battery. *J. Power Sources* **2021**, *495*, 229795. [[CrossRef](#)]
21. Yuan, S.; Chang, C.; Yan, S.; Zhou, P.; Qian, X.; Yuan, M.; Liu, K. A review of fire-extinguishing agent on suppressing lithium-ion batteries fire. *J. Energy Chem.* **2021**, *62*, 262–280. [[CrossRef](#)]
22. Xu, J.; Guo, P.; Duan, Q.; Yu, X.; Zhang, L.; Liu, Y.; Wang, Q. Experimental study of the effectiveness of three kinds of extinguishing agents on suppressing lithium-ion battery fires. *Appl. Therm. Eng.* **2020**, *171*, 115076. [[CrossRef](#)]
23. Meng, X.; Jiang, L.; Duan, Q.; Wang, S.; Duan, P.; Wei, Z.; Zhang, L.; Jia, Z.; Jin, K.; Wang, Q. Experimental study on exploration of optimum extinguishing agent for 243 Ah lithium iron phosphate battery fires. *Process. Saf. Environ. Prot.* **2023**, *177*, 138–151. [[CrossRef](#)]
24. GB 38031-2020; Electric Vehicles Traction Battery Safety Requirements. State Administration for Market Regulation, Standardization Administration of the People’s Republic of China: Beijing, China, 2020.
25. COMSOL Multiphysics® v. 6.3. COMSOL AB, Stockholm, Sweden. Available online: <https://www.comsol.com/> (accessed on 20 December 2024).

26. Wang, Y.; Kalinina, A.; Sun, T.; Nowack, B. Probabilistic modeling of the flows and environmental risks of nano-silica. *Sci. Total. Environ.* **2016**, *545–546*, 67–76. [[CrossRef](#)]
27. Sakharova, A.; Kozlov, I.; Baydarashvili, M.; Petriaev, A. Reduction of negative impact on the geoenvironment using silica sol in road construction. *MATEC Web Conf.* **2019**, *265*, 06002. [[CrossRef](#)]

Disclaimer/Publisher’s Note: The statements, opinions and data contained in all publications are solely those of the individual author(s) and contributor(s) and not of MDPI and/or the editor(s). MDPI and/or the editor(s) disclaim responsibility for any injury to people or property resulting from any ideas, methods, instructions or products referred to in the content.